Tellus (1988), *40A*, 188–204

Baroclinic outbreak episodes in wavenumber domain

By HEINZ-DIETER SCHILLING, *Department of Meteorology, University of München, Theresienstr. 37, 8000 München 2, FRG*

(Manuscript received 1 January 1986; in final form 29 June 1987)

ABSTRACT

In contrast to the common definition of anomalous atmospheric flow by persistent and localized geopotential height anomalies, we define significant excursions from normal conditions by persistent anomalies of a single spectral energy conversion on a circumpolar scale. Whereas amplification of transient geopotential height or streamfunction anomalies generally involves a variety of possible processes and complex energetics, our approach defines strongly distorted energetics of a certain kind. With data covering 10 years (1967–1976), we study baroclinic energy conversions from zonal mean to zonal wavenumber m available potential energy, $C(A_z A_m)$, when these exceed the long-term average by more than a standard deviation for at least 3 consecutive days. During these episodes, called baroclinic outbreaks (BO), $C(A_m K_m)$ and the kinetic energy of wave m, K_m, are also large in all probability. Although short BO cases are frequent for all m, there is a secondary maximum of frequency at about 7 days for the ultralong wave $m = 2$. Composite energetics of BO's are presented, and a profound transformation of the 500 mb flow is shown for a long lasting $m = 2$ BO event.

1. Introduction

Anomalous atmospheric flow is commonly defined by persistent localized geopotential height anomalies (e.g., Dole, 1986) or even by some interesting synoptic feature (blocking). Subsequent analysis of these events by energetical means (see Hansen and Sutera, 1984; Schilling, 1986, Hansen and Chen, 1982; Fischer, 1984) suffer from large differences of the energetics between single blocking events. Certainly, flow patterns show the integral effect of different cooperating processes rather than being a reliable indicator of a well defined mechanism. Moreover, it can easily be shown that dynamics with very different characteristics build up similar synoptic patterns (e.g., Schilling, 1986). A more objective definition of the event to be analyzed was given in the studies of Tsay and Kao (1978a,b), Hansen (1986) and Itoh (1983). They investigated a set of amplification episodes related to one special zonal Fourier component or a group of them. Though such studies have contributed to our understanding of amplification episodes, the results cannot be easily interpreted in many cases (e.g. Itoh, 1983). Again, the energy input is generally quite complicated since many processes take part. In our study a further step was made by defining episodes characterized by a single extraordinary energy conversion. The study of these events is simplified since their energetical structure is strongly distorted by definition. Simultaneously, it is interesting to find the prevalent conditions leading to a very large single energy conversion.

As an example, we deal with episodes of vigorous baroclinic activity of zonal waves m called baroclinic outbreak episodes (BO). In this paper, the baroclinic activity of zonal wavenumber m is given by the evolution of the baroclinic conversions $C(A_z A_m)$ and $C(A_m K_m)$ and the corresponding growth of kinetic energy K_m. These quantities are averages over the depth of the troposphere and over a northern latitude belt [viz. definitions (6a)–(6c)] and were computed on a daily basis for 1967–1976. As usual, our computation of $C(A_m K_m)$ is a very rough estimate and a more reliable measure for baroclinic activity is given by $C(A_z A_m)$, which represents the baroclinic input in favour of the total energy of wave m. Parallel evolution of $C(A_m K_m)$ and $C(A_z A_m)$ was sometimes reported in the literature (e.g., Brown, 1969; Kubota, 1959). On a statistical basis, they are correlated less for small m (ultralong waves) than for synoptic scales (e.g., $m = 5,6,7$). However, persistent large valued $C(A_z A_m)$ conversions are indicative for large $C(A_m K_m)$, leading to a better than normal correspondence between the two (Schilling, 1987). In this sense, we consider waves m with large input $C(A_z A_m)$ to be baroclinically active if K_m grows fast at the same time.

2. Baroclinic activity of ultralong waves

Daily records of the baroclinic conversions $C(A_z A_m)$ for $m = 2,3$ or 4 (averaged over the troposphere and latitudes north of 40°N) are noteworthy, since they reveal that episodes of large baroclinic input from the zonal mean are more frequent than classical linear instability theories would have predicted (e.g. Hansen, 1986; Schilling, 1986). When these episodes are very long-lived the second conversion $C(A_m K_m)$ is also large in all probability (Schilling, 1987). It was this ultralong wave behaviour which has initiated this study. The theoretical background is given by the relationship between baroclinic activity of wave m and (linear) baroclinic instability. Certainly, baroclinic instability is simply a special case of baroclinic activity as confirmed by numerous linear or weakly nonlinear computations of $C(A_z A_m)$ and $C(A_m K_m)$ (e.g., Frederiksen, 1978; Gall, 1976; Brown, 1969; Smith, 1974). Linear or weakly nonlinear instability deals simply with initial perturbation amplitudes being very small, whereas baroclinic activity in general occurs at arbitrary perturbation amplitudes.

Ultralong waves are generally characterized by marginal baroclinic instability for initially small perturbation amplitudes. Even then, as noted by Bengtsson (1978), the wave purturbation amplitude oscillates and displays substantial growth from time to time although exponential growth is unimportant. A similar result is found by Farrell (1985) for synoptic scale waves. For fully nonlinear instability we have a different situation. If the initial ultralong wave phase configuration is favourable and the initial wave amplitude is sufficiently large, the above mentioned oscillatory development is more pronounced. In this case the initial evolution can be as strong as if large growth rates (in a linear sense) were controlling it (Schilling, 1984); simultaneous forcing by nonlinear wave-wave interactions strengthens this effect (Schilling, 1982). Therefore, vigorous baroclinic activity can be a manifestation of fully nonlinear baroclinic instability. This idea is illustrated by the following realistic example.

Fig.. 1 shows an episode of vigorous development of baroclinic conversion $C(A_z A_2)$ and Fig. 2 depicts the related evolution of kinetic energy of wave $m = 2$. The data source is described in Section 3. The conversion $A_2 \rightarrow K_2$, $C(A_2 K_2)$, is also shown in Fig. 1 (dotted curve). An effort was made to predict the evolution of $K_2(t)$ 5 days in advance using a regression model, involving only $K_2(t_0)$ and $C(A_z A_m)(t)$ as inputs (Fig. 2, dashed curve). The dotted curve was derived by a similar approach except for considering the conversions stemming from nonlinear wave-wave interaction as an additional input. The model reads (for symbols not explained in the text see Appendix A)

$$\begin{aligned} j > 1: \hat{K}_2(t_0 + \Delta t \cdot j) &= \exp(-k\Delta t) \cdot \hat{K}_2(t_0 \\ &+ (j-1) \cdot \Delta t) + (\alpha/2) \cdot \{C(A_z A_2)(t_0 + j \cdot \Delta t) \\ &+ \exp(-k\Delta t/2)\, C(A_z A_2)(t_0 + [j-1] \cdot \Delta t)\} \\ &+ (\gamma/2)\{\ldots\} \\ j = 1: \hat{K}_2(t_0 + \Delta t) &= \exp(-k\Delta t) \cdot K_2(t_0) \\ &+ (\alpha/2) \cdot \{C(A_z A_2)(t_0 + \Delta t) + \exp(-k\Delta t/2) \\ &\times C(A_z A_2)(t_0)\} \\ &+ (\gamma/2)\{\ldots.\};\ K_2(t) = \hat{K}_2(t) + r(t) \end{aligned} \tag{1a}$$

The residue $r(t)$ is assumed to be uncorrelated with $\hat{K}_2(t)$; α, γ and k have to be specified by least square methods.

Both models (with and without nonlinear wave-wave interaction) are able to predict the above normal development of K_2 during this episode (see monthly mean and σ_K for reference). However, the prediction by $C(A_z A_2)$ plus nonlinear interactions is considerably better than by $C(A_z A_2)$ alone, especially at the early stages. Moreover, we speculate that these interactions are able to enhance the baroclinic activity simply by inducing higher 'initial' perturbation

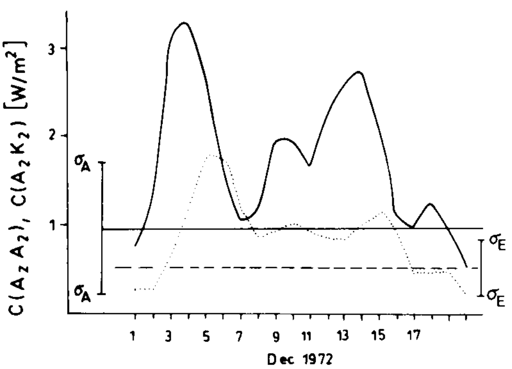

Fig. 1. Baroclinic energy transformation $C(A_zA_2)$, averaged over $1000\ \text{mb} \geq p \geq 300$ mb and $40°\text{N} \leq \varphi \leq 85°\text{N}$ for zonal wavenumber $m = 2$ (solid line) and the period Dec. 1–Dec. 18, 72. Dotted curve: $C(A_2K_2)$. Long-term monthly averages of both fluxes (upper solid bar: $C(A_zA_2)$, Broken: $C(A_2K_2)$) and standard deviations are indicated (σ_A for $C(A_zA_2)$, σ_E for $C(A_2K_2)$).

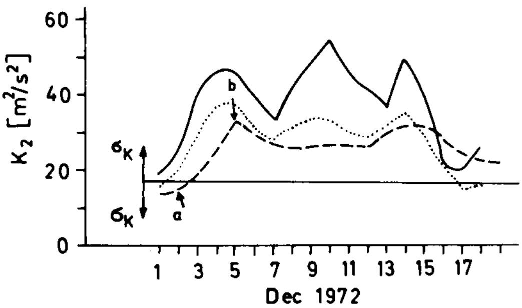

Fig. 2. Kinetic energy K_m for $m = 2$. Averaging domain and period as in Fig. 1. Solid line: observation. Dashed: predictions derived from the regression model (1a) for 5 days in advance using $C(A_zA_2)$. Dotted: predictions from (1a), except for using (CA_zA_2) plus nonlinear wave-wave-interactions. Symbols a, b denote the part of the curve which should be explained by the linear model (1b). Long-term monthly mean of K_2 (bar) and standard deviation σ_K are indicated.

amplitudes for the next time step. Nevertheless, $C(A_zA_2)$ alone forces K_2 to grow vigorously from (a) to (b) (see Fig. 2, dashed curve) and we will try to explain this growth by a linear model with a standing wave $m = 2$ as part of the basic flow. Details of this linear model are given in Appendix C, since they are of minor importance here, and we focus on the most unstable mode with normalized initial amplitude a_0 and realistic e – folding time T_e:

$$K_2 = K_{2,st} + K_2'; \quad K_2' = K_{2,st} \cdot \{2a_0 \exp(t/T_e) + a_0^2 \exp(2t/T_e)\};$$
$$a_0 = \{K_2(t_0)/K_{2,st}\}^{1/2} - 1. \tag{1b}$$

Initially, $K_2(t_0)$ at point (a) is relatively large and the 'linear' perturbation takes only a small fraction of it. Accordingly, we set the initial perturbation kinetic energy K_2' to be 30% of that of the standing wave part of the basic flow $K_{2,st}$, resulting in $K_2(t_0) = 1.3\ K_{2,st}$. After (C4) in Appendix C, we need $T_e = 2.45$ days or less to explain the increase of K_2 from (a) to (b). Of course, this T_e is unreasonable for m = 2 although the initial perturbation energy is as large as 30% of $K_{2,st}$ and therefore at the border to the nonlinear regime. In order to obtain *e*-folding times T_e of about 8 days, found by Sasamori and Youngblut (1981) under fairly realistic conditions for $K_{2,st}$, we need an initial pertubation kinetic energy amounting to $15 \times K_{2,st}$. This virtually means $K_2(t_0) \approx K_2'(t_0)$ and is not consistent with the small perturbation assumption. The fully nonlinear nature of vigorous baroclinic activity in this case is also indicated by the simultaneous fast decay of K_2 and $C(A_zA_2)$ at the end of the episode. This behaviour is not explained by weakly nonlinear theories. On the other hand, vigorous baroclinic activity of wave $m = 2$ does not always end in as fast a decay of K_2 as in this case. More details on this item will be given in a forthcoming paper.

The following study is concentrated upon definition and statistics of wave m events with vigorous development like that in the example. In Section 4, we define BO episodes and give a statistical background with historical data of a 10-year period (1967–1976). In Sections 5 and 6, we describe flow transformation for BO events of long durations.

We should stress the fact that in this study there is no reference to blocking activity from the outset. Nevertheless, some cases of long lasting BO in the ultralong wave range eventually evolve into a major blocking event.

3. Data and evaluation scheme

Daily northern hemisphere geopotential height data from the German Weather Service (DWD) is available at 1000 mb, 500 mb and 300 mb on a (λ, φ)—grid from $\varphi = 15°$N to $\varphi = 85°$N with increments $\Delta\lambda \times \Delta\varphi = 10° \times 5°$ for the years 1967–1976. Each height field Z was decomposed in zonal Fourier-components:

$$Z(\lambda, \varphi_i, t) = \sum_m^M \{a_m(\varphi_i, t) \cos(m\lambda) + b_m(\varphi_i, t) \sin(m\lambda)\} \tag{2}$$

$$M = 12; \quad \varphi_i = \varphi_0 + i \cdot \Delta\varphi \leqq \varphi_{16}; \quad i = 0, \ldots, 16$$

With data of 3 height fields we can form 2 thickness fields $h = g\Delta z$ after

$$\Delta\Phi/\Delta p = h/\Delta p \approx 1/\varrho = \alpha \tag{3}$$

They represent the model temperature of our quasi-geostrophic data evaluation scheme. According to simple quasi-geostrophic models we assume the static stability to be dependent on time only:

$$\sigma_0(t) = [-(1/\varrho)\partial \ln \Theta/\partial p]_{15°}^{85°} \tag{4a}$$

The symbol $[\,]_{\varphi_A}^{\varphi_B}$ denotes an average over the latitude band $\varphi_A \leqq \varphi \leqq \varphi_B$ and the depth of the troposphere:

$$[\mathrm{Y}]_{\varphi_A}^{\varphi_B} = \sum_{j=1}^{J} (\Delta p_j/p_B) \times \left\{ \sum_{k=A}^{B} \bar{Y}(\varphi_k) \cos\varphi_k \Big/ \sum_{k=A}^{B} \cos\varphi_k \right\} \tag{b}$$

($J = 2$ for baroclinic and $J = 3$ for barotropic expressions).

We evaluate (4a) according to

$$-(1/\varrho)\partial \ln \Theta/\partial p = c_v/(c_p \cdot p)\, \partial\phi/\partial_p + \partial^2\phi/\partial p^2, \tag{5}$$

with ϕ quadratically interpolated between the available data levels 300 mb, 500 mb, and 1000 mb.

Next we compute the energy conversion from zonal mean available potential energy (APE) into that of zonal wave m averaged over the latitudinal belt $40° \leqq \varphi \leqq 85°$ N, together with the kinetic energy of wave m:

$$C(A_z A_m) = -(p_B/g\sigma_0) \left[\frac{h_m}{\Delta p_j^2} \times \{J(\psi', \bar{h})|_m + J(\bar{\psi}, h')|_m\} \right]_{40°}^{85°} \tag{6a}$$

$$K_m = (p_B/g) \left[\frac{1}{2} \left\{ \frac{\partial\psi_m}{a \cdot \cos\varphi\, \partial\lambda} \right\}^2 + \frac{1}{2} \left\{ \frac{\partial\psi_m}{a\, \partial\varphi} \right\}^2 \right]_{40°}^{85°} \tag{6b}$$

We have to consider the second baroclinic conversion, too:

$$C(A_m K_m) = (p_B/g)\, [f_0 \cdot \omega_m \cdot \partial\psi_m/\partial p]_{40°}^{85°} \tag{6c}$$

The ω-field can be computed from our data. The procedure for estimating ω and heating simultaneously from or data is given in Appendix B. Since the diabetic heating is not known a priori and the vertical resolution is poor we have to be aware of severe errors of the ω-estimates with our data. In Table 1 we have collected the long term winter means of $C(A_z A_m)$, $C(A_m K_m)$ as computed from our data. The averages are comparable to recently reported results which are related to only a few winters. However, the $C(A_m K_m)$ estimates seem to be systematically too low. Indeed, in deriving our daily conversion rates we were forced to interpolate the Φ or ψ-fields in time, because tendencies of Φ or ψ are involved. After Oerlemans (1981) this gives rise to a considerable reduction of covariance of ω_m and $\partial\Phi_m/\partial$p (up to 40%). This may explain our low averages in Table 1b. Since variances of $C(A_m K_m)$-estimates display the same failure, only conversions $C(A_m K_m)$, normalized with their standard deviation, appear to be meaningful.

4. Statistics and baroclinic outbreak definition

4.1. Probabilities

To eliminate long term trends and seasonal variability we transform our time series $M_m = C(A_z A_m)$ according to $N_m = M'_m/\sigma_m$, with $\langle M_m \rangle$ denoting a long term monthly mean, $M'_m = M_m - \langle M_m \rangle$ an anomaly and $\sigma_m = \sqrt{\langle (M'_m)^2 \rangle}$ the standard deviation. The transformed measure has unit variance and zero

Table 1. *Winter averages of baroclinic conversions* (W/m^2)

(a) $C(A_z A_m)$

Author (data source)	Averaging domain	Winter definition	1	2	3	4	5	6	7	8
							m			
Schilling (1987) northern belt (ECMWF)	45 → 85°N 300 → 1000 mb 3 winters	Nov. 20– Mar. 3 1980–83	0.66	0.79	0.89	0.46	0.41	0.31	0.21	0.14
This paper northern belt (DWD)	40 → 85°N 300 → 1000 mb 9 winters	Dec. 1– Feb. 28 1967–76	0.57	0.99	0.83	0.49	0.40	0.37	0.28	0.18
Schilling (1987) broad belt (ECMWF)	15 → 85°N 300 → 1000 mb 3 winters	Nov. 20– Mar. 3 1980–83	0.50	0.49	0.63	0.31	0.41	0.38	0.30	0.18
Tomatsu (1979) (NOAA, Nation. Weather Serv.)	25 → 75°N 100 → 925 mb 1 winter	Dec. 1– Feb. 28 1964/65	0.53	0.64	1.09	0.34	0.58	0.52	0.31	0.22

(b) $C(A_m K_m)$

Author (data source)	Averaging domain	Winter definition	1	2	3	4	5	6	7	8
							m			
Schilling (1987) northern belt	see Table 1a	see Table 1a	0.65	0.70	0.60	0.44	0.45	0.38	0.32	0.24
This paper northern belt	see Table 1a	see Table 1a	0.29	0.57	0.27	0.19	0.17	0.17	0.13	0.08
Schilling (1987) broad belt	see Table 1a	see Table 1a	0.46	0.40	0.42	0.26	0.35	0.35	0.33	0.24
Chen et al. (1981) (NMC)	20 → 85°N 100 → 1000 mb 1 winter	Dec. 1st– Jan. 31st 1977/78	0.23	0.37	0.30	0.25	0.30	0.33	0.22	0.23
Tomatsu (1979) broad belt	see Table 1a	see Table 1a	0.43	0.28	0.51	0.37	0.38	0.29	0.27	0.22

mean. Other time series, e.g., K_m, are transformed in the same manner.

Fig. 3 shows the frequency distribution of the transformed measure $N' = M'/\sigma$ for $m = 2$. For comparison M'/σ is also shown for $m = 3$, $m = 7$. Note that positive values of unnormalized M_m are more frequent than negative ones (see Schilling, 1987). The frequency distributions of N'_m for different m are similar. There is neither a secondary peak for large values of N'_m nor a 'plateau' in the vicinity of $(1-2) \times \sigma$.

Another situation appears with the integrated above-normal baroclinic input for nearly all m. This parameter $\sum|$ is the sum of normalized $C(A_z A_m)$ beginning with a crossover to above-normal values and ending with the crossover to below-normal values. The frequency distribution of $\sum|$ shows a secondary peak or plateau for $\sum| = 2.5 - 4$ and another one for $\sum| = 6 - 8$ (not shown). This finding may indicate that there are two modes of baroclinic activity: a series of small fast fluctuating 'kicks' with some major 'kicks'

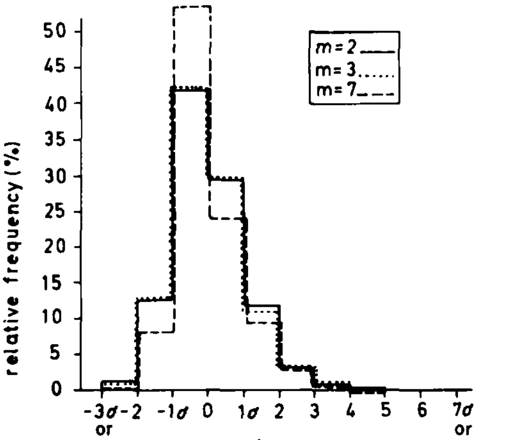

Fig. 3. Frequency distribution of standardized baroclinic energy conversion N'_m for $m = 2$ (definition see text; solid curve). Dotted: Same distribution, except for $m = 3$, dashed: for $m = 7$.

imbedded (see also Schilling, 1987). As noted in the Introduction, situations with large M'_m (greater than σ_m, say) are of special interest for ultralong waves. For example, the probability of $M'_2/\sigma_2 > 1$ is about 14.9% and slightly higher than for other wavenumbers (Table 2).

Events with $N'_m > 1$ for 3 days in row are relatively rare. However, they are much more frequent than those given by 3 independent choices out of a set of normalized Gaussian distributed random variables (denoted by the term 'stochast.' in Table 2). The frequency of such events decreases with m as one can expect from scale-wise persistency characteristics.

On the other hand, probabilities do not say much about the underlying dynamics and this point will be discussed next.

4.2. Definition of baroclinic outbreaks

In the remainder we are interested in persistent large values of $N' > 1$, say. Therefore the definition of a BO period related to m is:

(a) The basic period of BO consists of at least $P_0 = 3$ consecutive days with $N'_m > N_0 = 1$.

(b) In addition, preceding or following days with $N'_m > 0.75\ N_0$ belong to the BO period. (7)

(c) If there are preceding or following days with $N'_m > N_0$ being separated from the BO period after (a) and (b) they are added to the BO period provided that the separation period consists of maximal 3 days with $N'_m > 0.20\ N_0$; the separation days belong to the BO period too.

This definition is admittedly arbitrary as to the threshold values N_0, P_0, but it is intended to match the observed complex morphology of the outbreaks (compare with Fig. 1). The number of cases according to (7) varies considerably with N_0, P_0, as does the duration of many events. On the other, hand long lasting major events are nearly unaffected by variations of N_0, P_0 within reasonable limits. In the following we will summarize the reasons for adopting our values $P_0 = 3$ days and $N_0 = 1$.

First let us consider P_0. Naturally, P_0 should correspond to the typical time scale of N'_m.

Table 2. *Probabilities for different events related to normalized $C(A_z A_m)$; definitions see text*

Event:	1 day with $N' \geq 1$	3 days in row with $N' \geq 1$		BO days after (7)
Wavenumber m	Observed	Observ.	Stochast.	Observed
1	14.8%	5.3%	0.32%	12.2%
2	14.9%	5.2%	0.33%	12.6%
3	14.8%	3.6%	0.32%	9.1%
4	14.3%	3.0%	0.29%	7.4%
5	13.1%	2.7%	0.22%	7.0%
6	13.3%	2.5%	0.24%	6.8%
7	14.0%	2.3%	0.27%	6.8%
8	13.9%	2.6%	0.27%	6.3%

Autocorrelations of normalized $C(A_z A_m)$ with time lag 1 day give typical e-folding times in the range of 3.8 days ($m = 1$) or 3.4 days ($m = 2$) to 1.5 days ($m = 7,8$). Therefore P_0 should not be less than 2 days. If $P_0 = 3$ days or more there has to be a powerful process to maintain this energy conversion against dissipative processes. If P_0 is too large it limits the number of BO-days to inconveniently small values. A fair compromise would be $P_0 = 3$ days. Secondly, lowering of N_0 would increase the number of BO-days. If we are solely interested in a large set of BO-events we just have to set N_0 far below 1.0. On the other hand, by (7) we want to extract extraordinary periods out of the normal course of events. Extraordinary baroclinic activity of wave m is not only given by large $C(A_z A_m)$ but should be accompanied by large $C(A_m K_m)$ and K_m, too. We have recorded the frequency distributions of normalized $C(A_m K_m)$ and K_m for all BO-days according to (7) for $P_0 = 3$ days and two $N_0 = .6$, 1.0. The results are shown for $m = 2$, 3 and 7 in Fig's 4a–f. It turns out that the distortion of the frequency distributions becomes increasingly sharp with increasing threshold N_0. Now we are sure that larger N_0 will define periods with larger baroclinic activity and better correlated energetics. Again, in this respect $N_0 = 1$ is a fair compromise, since the total number of BO-days with normalized $C(A_m K_m)$ or $K_m \geqq 1$ minus those with $C(A_m K_m)$ or $K_m \leqq 0$ is maximized then. This means that the strong distortion of the relevant frequency distributions of $C(A_m K_m)$ and K_m is not yielded at the expense of the number of BO-days. It should be noted that $N_0 = 1$ was also adopted by Itoh (1983) in his definition of amplification periods.

5. Statistics on events

5.1. *Frequency of events, duration and kinetic energy spectra*

According to definition (7), there are several BO cases for any single m during the period 1967–1976. The total number of BO events and BO days for different waves m is given in Table 3a; the relative frequency of BO days is shown in Table 2 (last column). Some examples of the frequency of their durations are given in Fig. 5. Very persistent BO's prevail for $m = 2,3$. For shorter wavelengths (larger m), the duration tends to be much shorter. Of course, we are interested in long-lasting events since they should transform the flow by rapid amplification of BO-wave m. Again, the ultralong wave $m = 2$ serves as an example and we collect its ultra-persistent cases (duration longer than 6 days) in Table 3b. Seasonal stratification reveals that $m = 2$ BO's are not as frequent in summer as in winter.

As to the coincidence of events for different m, Fig. 6 shows that no rule for any systematic combination of m's is evident. We note that BO's tend to be spread over the winter months shown, with only a slight tendency towards clustering. It is understood that time averages of strongly developing energies are less meaningful than those derived from stationary time series. Nevertheless, we want to give an overall impression of the spectral structure of normalized kinetic energy prevalent in BO's (Fig. 7). The signature of strong baroclinic activity during BO's is recognized by the fact that the wave M, for which the BO event is recorded, tends to be the dominant one in the spectrum, K_m, $m = 1, \ldots 8$. Sideband waves are generally below normal (= zero) during ultralong wave BO's. Moreover, during $m = 1,3$ events the synoptic scale (typically $m = 7,8$) appears to be below normal. A similar case-averaged spectrum can be derived for the conversions $C(A_m K_m)$ and $C(A_z A_m)$ (not shown). Again the conversions for the BO-wave are strongly pronounced whereas the side-band wave conversions tend to be below normal. When the BO-wave is an ultralong one, the baroclinic activity of the other wave packets appear to be somewhat suppressed (see also Hansen, 1986, and Schilling, 1986).

5.2. *Energy diagrams of baroclinic outbreaks*

Baroclinic activity is only one part of the driving of the wave energy. Therefore we are interested in a more complete energy flux diagram during BO events revealing other processes favourable for the BO dynamics. At least two processes are often suspected to play a special role in ultra-long wave amplification episodes: diabatic heating (via SST-anomalies) and nonlinear wave-wave interaction with synoptic scales. The latter was successful in forcing blocking-like patterns formed by amplified

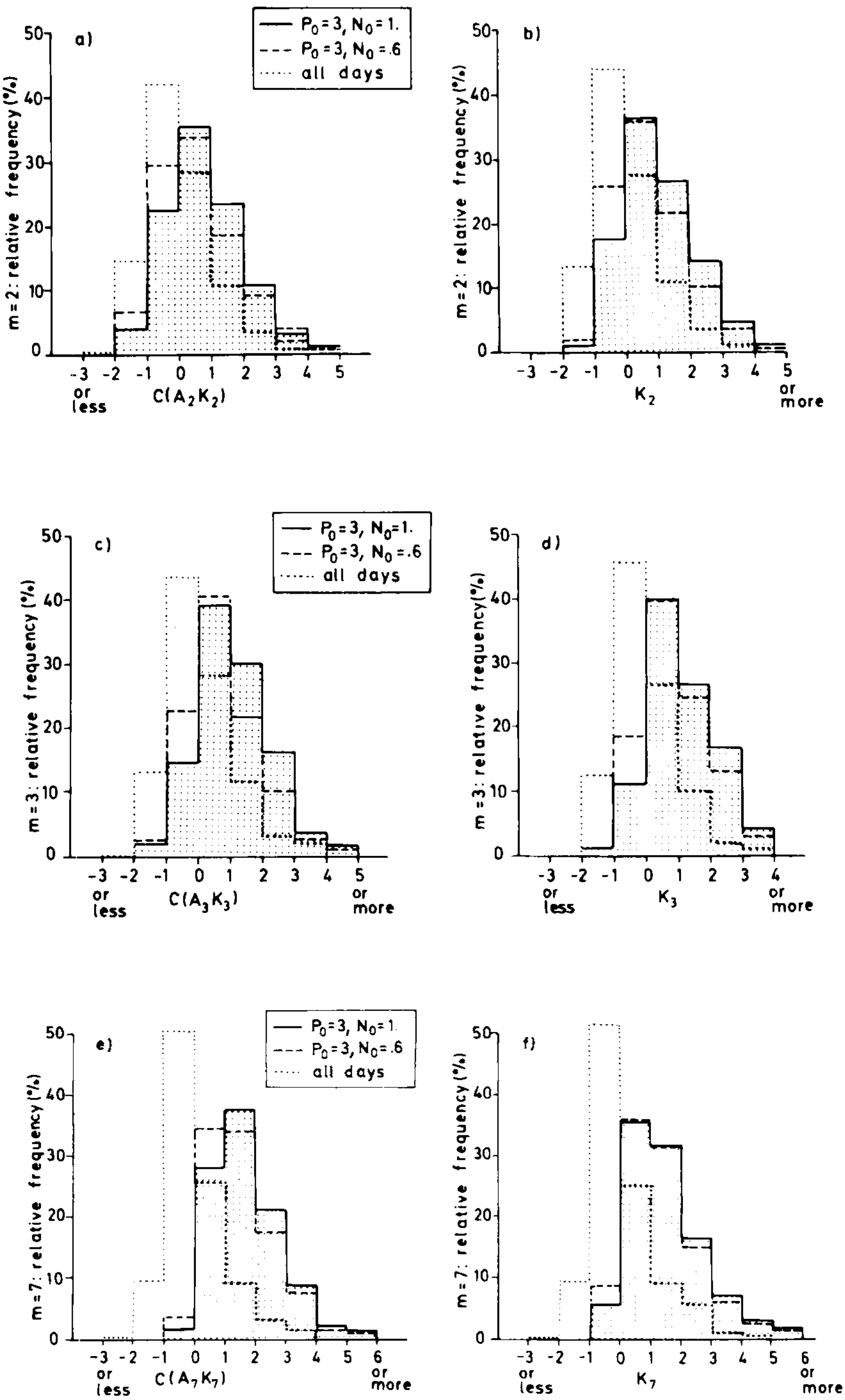

Fig. 4. Frequency distribution of different parameters and waves m restricted to BO-days after (7) but for $N_0 = 0.6$ (dashed) and 1.0 (solid curve). Reference distribution for all days is dotted. (a) $C(A_2K_2)$, (b) K_2, (c) $C(A_3K_3)$, (d) K_3, (e) $C(A_7K_7)$, (f) K_7.

ultralong waves in a simple barotropic model (Metz, 1986). Numerical tests of the hypothesis that SST-anomalies can force ultralong waves to larger than normal energy levels, gave positive results (Simpson and Downey, 1975; Chen and Shukla, 1983). However, in these simulations the model SST-anomalies have to be slightly beyond the upper bound of observed values or even higher to yield significant signals.

We complete the usual quasi-geostrophic energy cycle by adding the above mentioned inputs as well as other possible candidates. These are the conversion from zonal mean to wave kinetic energy K_m [recall definition (4b)]:

$$C(K_z K_m) = (p_B/g)$$
$$\times \left[\bar{u} \frac{1}{a^3 \cos^2 \varphi} \frac{\partial}{\partial \varphi} \left\{ \cos \varphi \frac{\partial \psi_m}{\partial \lambda} \frac{\partial \psi_m}{\partial \varphi} \right\} \right]_{40^\circ}^{85^\circ},$$

Table 3(a). *Total number of BO events and BO days for the period 1967–1976*

Wavenumber	1	2	3	4	5	6	7	8
No. of cases	67	73	68	63	60	53	56	47
No. of days	444	460	332	269	256	248	246	230

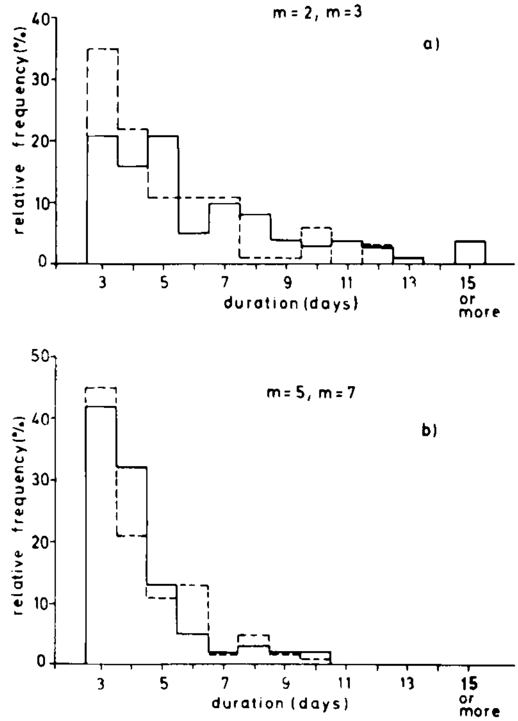

Fig. 5. Frequency of the duration of BO events; (a) for $m = 2$ (solid) and $m = 3$ (dashed), (b) for $m = 5$ (solid) and $m = 7$ (dashed).

Table 3(b). *BO cases for m = 2 with durations longer than 8 days*

1. Winter cases (Nov.–Apr.): 18		2. Summer cases (May–Oct.): 10	
Dates	duration (days)	Dates	duration (days)
Feb. 12–Feb. 21 '67	10	Jul. 26–Aug. 1 '67	7
Feb. 26–Mar. 7 '67	10	May 8–May 14 '69	7
Apr. 1–Apr. 7 '67	7	Jul. 11–Jul. 19 '69	9
Nov. 3–Nov. 13 '67	11	Sep. 16–Sep. 30 '69	15
Jan. 9–Jan. 17 '69	9	Jun. 7–Jun. 14 '70	8
Nov. 23–Nov. 29 '69	7	Oct. 24–Oct. 31 '70	8
Jan. 3–Jan. 9 '70	7	May 3–May 10 '72	8
Apr. 14–Apr. 21 '70	8	Jul. 5–Jul. 12 '73	8
Jan. 2–Jan. 13 '71	12	Aug. 6–Aug. 12 '75	8
Jan. 30–Feb. 8 '72	10	Oct. 16–Oct. 26 '76	11
Dec. 2–Dec. 15 '72	14		
Jan. 3–Jan. 14 '74	12		
Feb. 4–Feb. 13 '74	10		
Mar. 7–Mar. 24 '74	18		
Dec. 17–Dec. 24 '74	8		
Jan. 22–Feb. 3 '75	13		
Nov. 3–Nov. 12 '76	10		
Dec. 2–Dec. 12 '76	11		

nonlinear wave-wave-interaction with scales $m > 5$ as participants, for kinetic energy as well as APE,

$$\mathrm{BTPLS}_m = (p_B/g)[\psi_m J(\psi_{1-5}, \nabla^2\psi_{6-12})|_m + \psi_m J(\psi_{6-12}, \nabla^2\psi')|_m]_{45^\circ}^{80^\circ}$$

$$\mathrm{BCLLS}_m = -(p_B/g\sigma_0) \times \left[\frac{h_m}{\Delta p_j^2}\{J(\psi_{1-5}, h_{6-12})|_m + J(\psi_{6-12}, h')|_m\}\right]_{40^\circ}^{85^\circ}$$

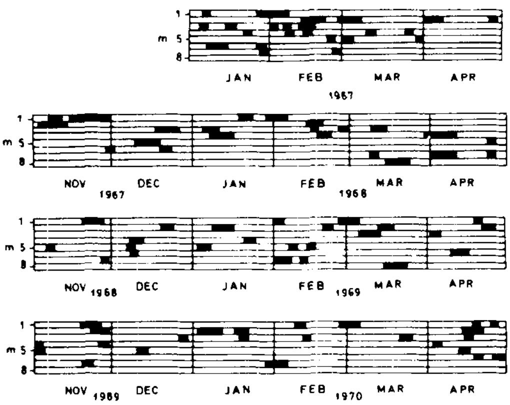

Fig. 6. Selected winter periods with BO's of different m indicated by thick solid bars. First line stands for $m = 1$, second line for $m = 2$, etc.

nonlinear wave-wave-interaction within the wavegroup $1 \leq m \leq 5$, for kinetic energy as well as APE,

$$\mathrm{BTPLL}_m = (p_B/g)[\psi_m J(\psi_{1-5}, \nabla^2\psi_{1-5})|_{m\neq 0}]_{45^\circ}^{80^\circ}$$

$$\mathrm{BCLLL}_m = -(p_B/g\sigma_0) \times \left[\frac{h_m}{\Delta p_j^2}\{J(\psi_{1-5}, h_{1-5})|_{m\neq 0}\}\right]_{40^\circ}^{85^\circ}$$

the generation term ($\mathrm{d}Q_m/\mathrm{d}t$ is heating),

$$G_m = (p_B/g\sigma_0) \times \left[\frac{h_m}{\Delta p_j}\mathrm{d}H_m/\mathrm{d}t\right]_{40^\circ}^{85^\circ}; \quad \mathrm{d}H_m/\mathrm{d}t = (R\mathrm{d}Q_m/\mathrm{d}t)/(p\cdot c_p)$$

and boundary fluxes (others are already incorporated in the nonlinear interaction terms);

$$\mathrm{BOUND}_m = (p_B/ga^2) \times \left\{\left[\cos(85^\circ)\left(\psi_m \frac{\partial^2\psi_m}{\partial t\,\partial\varphi}\right)\right]_{85}^{85^\circ} - \left[\cos(45^\circ)\left(\psi_m \frac{\partial^2\psi_m}{\partial t\,\partial\varphi}\right)\right]_{45^\circ}^{45^\circ}\right\}$$

Daily energy parameters for a single case were condensed by forming non-overlapping 3 day-averages (or alternatively 2 days-averages if not

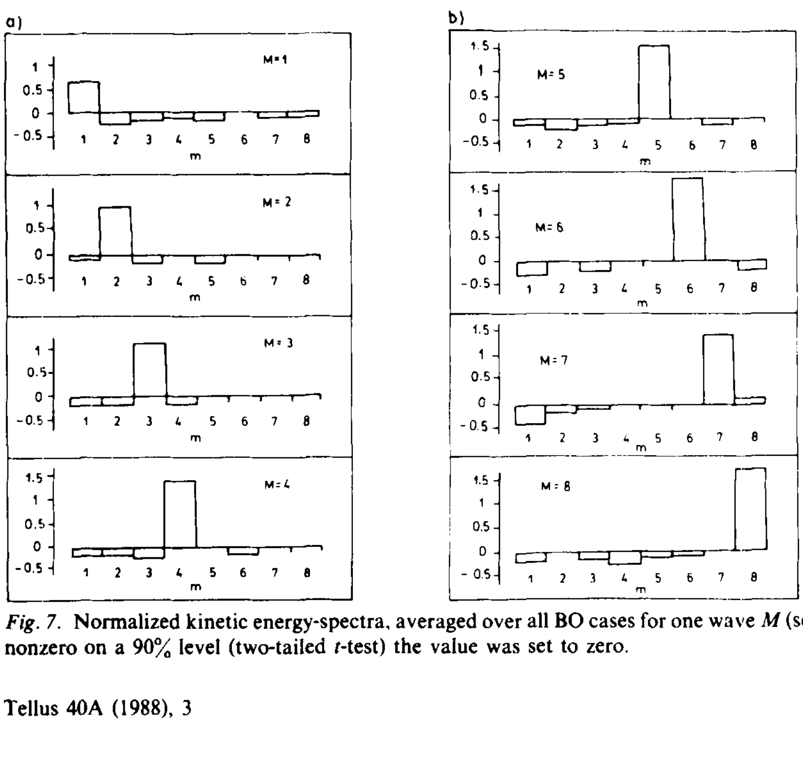

Fig. 7. Normalized kinetic energy-spectra, averaged over all BO cases for one wave M (see label). If not significantly nonzero on a 90% level (two-tailed t-test) the value was set to zero.

otherwise possible). Therefore the number of degrees of freedom equals the number of cases considered for one of the Figs 8a–f. The only exception is the diagram for the middle part of ultra-persistent BO episodes (Fig. 8e, solid arrows); here we have 31 degrees of freedom but 13 cases. Normalized values are given in Figs 8a–f whenever significantly different from zero (with respect to two-tailed t-testing and 10% error probability).

First we collect the time and case-average for $m = 2$ BO's lasting 3 days (Fig. 8a). The energy of $m = 2$ is considerably above normal (= zero) as is the case for $C(A_zA_2)$. On the other hand, $C(A_2K_2)$ is positive but too small. In a statistical sense it cannot be distinguished from zero (= average) on a 90%-level. Nonlinear interactions with other waves tend to pile up K_2 whereas interaction with zonal mean flow tends to be a sink for K_2. Other energy conversions appear to be nearly normal.

Next, $m = 2$ BO's lasting 4–6 days are given in Figs 8b,c. Also in these cases the energy of $m = 2$ is above normal. The main energy flow is as usual given by $A_z \rightarrow A_2 \rightarrow K_2$, but with usually large energy conversions. During the first half of the episodes, nonlinear interaction within the long wave

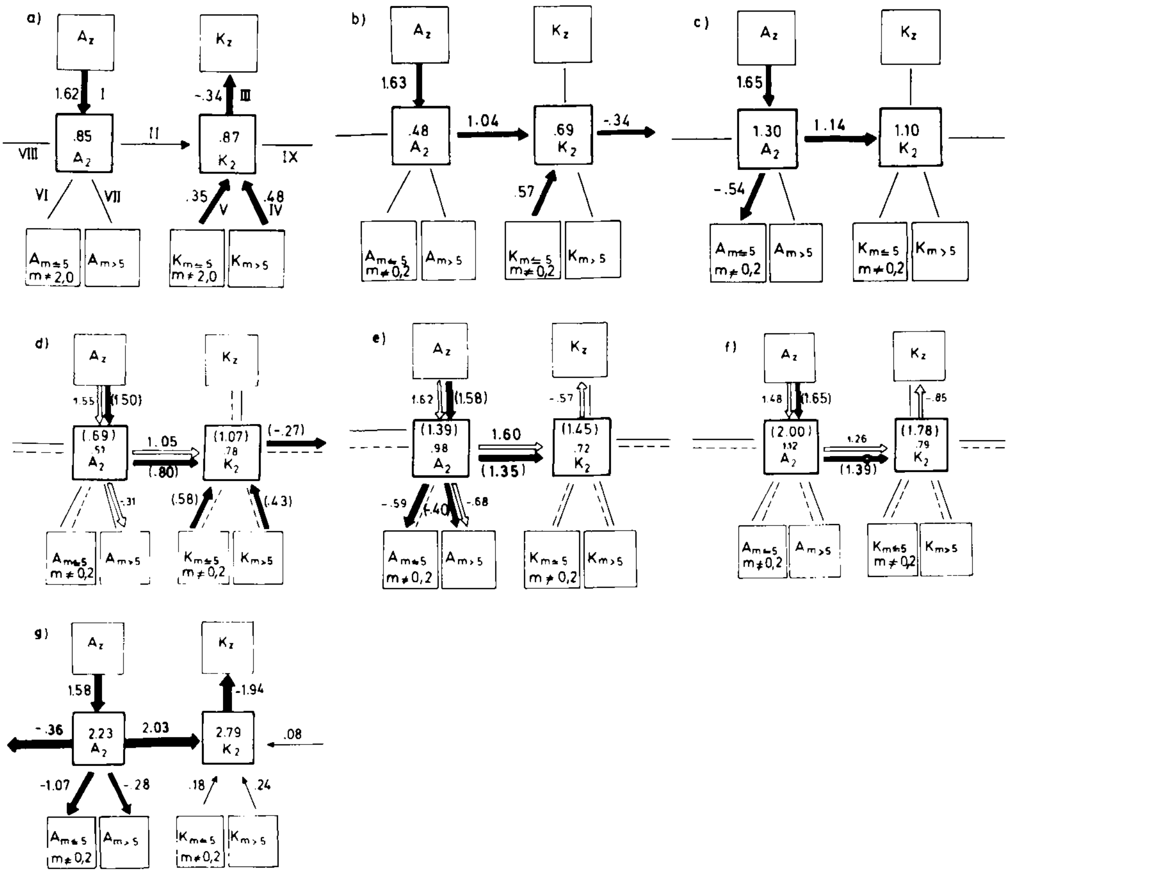

Fig. 8. Case averaged energy diagrams for $m = 2$ BO events of different durations (a) Duration 3 days. The normalized conversions are: I = $C(A_zA_2)$, II = $C(A_2K_2)$, III = $C(K_zK_2)$, IV = BTPLS$_2$, V = BTPLL$_2$, VI = BCLLL$_2$, VII = BCLLS$_2$, VIII = G_2, IX = BOUND$_2$. (b) The first half of events lasting 4–6 days. (c) The second half of events lasting 4–6 days. (d) The first 3 days of events lasting 7–9 days (open arrows) and of ultra-persistent cases lasting 10–18 days (solid arrows). (e) Averages over the BO period except for the first and last 3 days: duration 7–9 days (open arrow), duration 10–18 days (solid arrows). (f) The last 2 or 3 days of events lasting 7–9 days (open arrows) and 10–18 days (solid arrows). (g) The single case (see Introduction) Dec. 2–Dec. 15, 1972.

packet feeds the BO-wave. During the second half this process ceases to be effective and causes a loss of APE instead. In Figs 8d–f we collect the results for BO's with duration 7–9 days (open arrows) and duration 10–18 days (solid arrows). As before, the energies of $m = 2$ and the energy flow $A_z \rightarrow A_2 \rightarrow K_2$ are above normal. At later stages of the development, $C(K_z K_2)$ turns out to be a sink for K_2. Again, in this case of ultra-persistent BO's, nonlinear wave-wave interactions put energy into the BO-wave during the first 3 days, but boundary fluxes counteract that process moderately. Nonlinear wave-wave interactions related to APE appear to be a sink for A_2.

Summarizing the results we find: (i) A_2, K_2 and the energy flow $A_z \rightarrow A_2 \rightarrow K_2$ are developed well above normal. These parameters are describing the baroclinic activity of $m = 2$. (ii) Nonlinear barotropic wave-wave interaction serves as subsidiary process for the amplification of K_2 at the early stage of BO. Later on this process is no more important on the average. Besides the primary baroclinic activity this is the only mean energy source for K_2. Here we have another

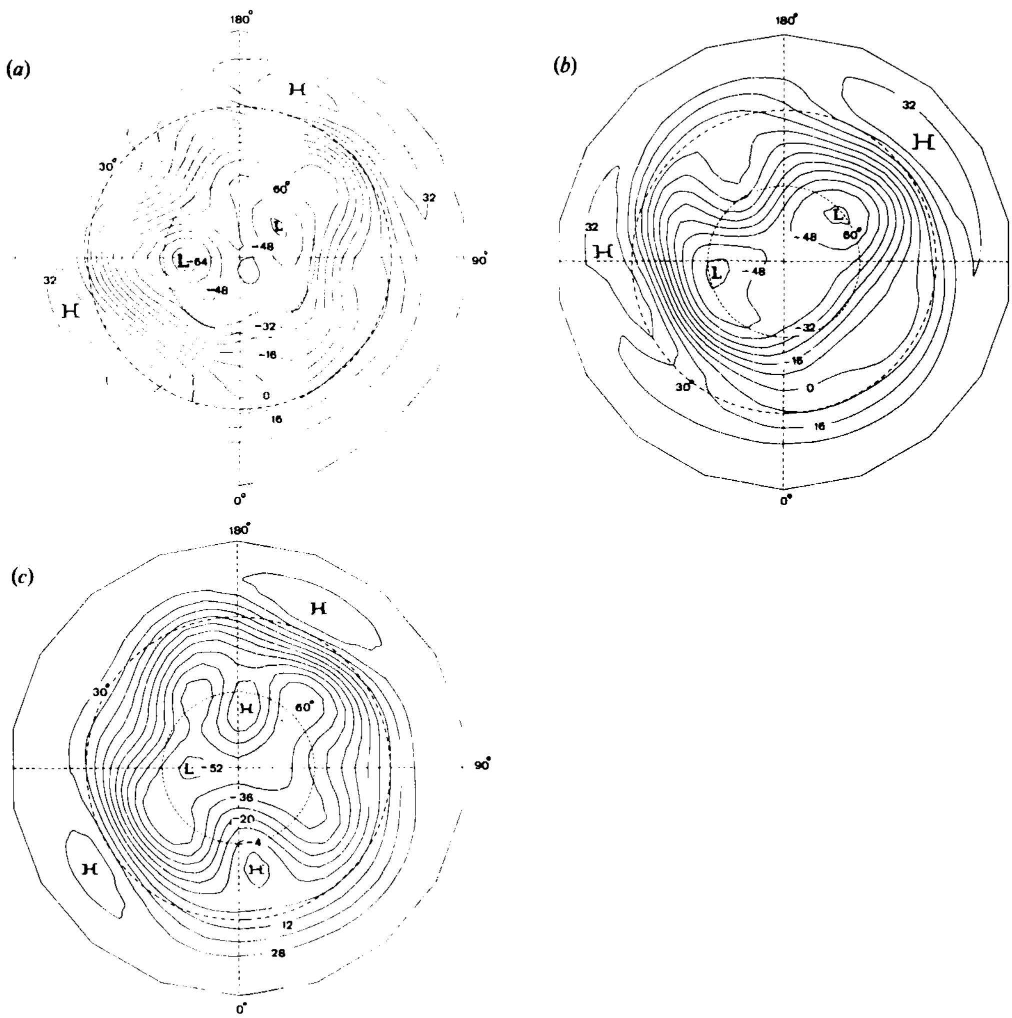

Fig. 9. (a) ψ at 500 mb averaged over 5 days before the onset of the single case Dec. 2–Dec. 15, 1972. (b) The average over the 5 days: Dec. 8–Dec. 12, 1972. (c) The average over the 5 days after the BO period.

indication for the fact that we are not dealing with initially small perturbations growing exponentially at early stages of the events. (iii) Nonlinear baroclinic wave-wave interaction, related to A_2, always tends to diminish APE of A_2, especially at later stages of longer BO's. (iv) $C(K_z K_2)$ appears to be a sink for K_2 at later stages of longer BO's. (v) Diabetic heating does not help to enhance the growth of A_2 and acts like a sink when anomalous.

Finally, we compare the energetics of the BO case, already discussed in Section 2, to the mean BO energy cycle for long lasting events. From Fig. 8g we see that this single case represents fairly well the middle stage of BO's lasting 10 days or more, although the energetic parameters are more pronounced.

6. Synoptic development

As an example, we will present the synoptic development of the single case already discussed above. To this end we compare 500 mb ψ-contours at the beginning, the middle and the end of that episode. Figs 9a,b,c reveal that the contours build up an ordered pattern eventually. Pronounced ridging develops into blocking highs although no reference to blocking was made in the BO definition. At the end of the BO a dominant wave m = 2 structure north of 30°N is clearly seen. Note that the BO definition uses energy parameters related to latitudes north of 40°N!.

Positive $C(A_z A_m)$ implies that the temperature component of wave m always lags the pressure component in the troposphere, since only this phase relation is able to transport sensible heat northward and helps to decrease the meridional temperature contrast. For the BO example of Fig. 9 we show the harmonic dial of wave $m = 2$ (Fig. 10), related to the 500 mb geopotential height Φ_2 (55°N,t) and the 500/1000 mb thickness field $\tau_2 = (1/g)\ h_2(55°\mathrm{N},t)$. Each entry a_2, b_2, etc., is averaged over three consecutive days and the label indicates the center day of the averaging period. The correspondence with phase angles θ, θ^{T} is given by:

$$\Phi_2 = |\Phi_2| \cos(m\lambda - \theta_2); \quad \theta_2 = a\tan\{b_2/a_2\}$$

$$\tau_2 = |\tau_2| \cos(m\lambda - \theta_2^{\mathrm{T}}); \quad \theta_2^{\mathrm{T}} = a\tan\{b_{\tau,2}/a_{\tau,2}\}$$

The optimum phase difference $\theta_2 - \theta_2^{\mathrm{T}}$ is $\pi/2$ since the $m = 2$ heatflux is proportional to $|\Phi_2||\tau_2| \sin(\theta_2 - \theta_2^{\mathrm{T}})$. According to Fig. 10, we have $\theta_2 - \theta_2^{\mathrm{T}} > 0$ throughout the BO period, and $\sin(\theta_2 - \theta_2^{\mathrm{T}})$ attains approximately half the optimum at the early stages of development (Table 4, same averaging convention as for Fig. 10). Moreover, the growing wave $m = 2$ is nearly stationary (Fig. 10). A physical explanation of the

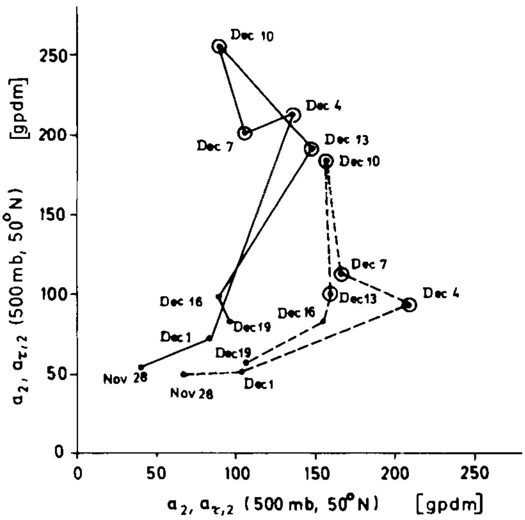

Fig. 10. Harmonic dial (a_2, b_2) for the single case Dec. 2–Dec. 15, 1972. A point represents a 3-day-average of a_2, b_2 or $a_{\tau,2}, b_{\tau,2}$ and is labelled with the center day of the averaging period. Solid: Φ at 500 mb and 55°N, dashed: $\tau = g^{-1} h$ in 55°N (h is the 500/1000 mb relative geopotential).

Table 4. Sine of the phase difference between $m = 2$ waves of Φ(55°N,t) and τ(55°N,t) for the case Dec. 2–Dec. 15 1972; BO days in *italics*.

Date	Nov. 28	Dec. 1	*Dec. 4*	*Dec. 7*	*Dec. 10*	*Dec. 13*	Dec. 16	Dec. 19
$\sin(\theta_2 - \theta_2^{\mathrm{T}})$	0.29	0.28	*0.55*	*0.47*	*0.36*	*0.37*	0.34	0.23

stationarity of $m = 2$ is beyond the scope of this paper. To this end, a model experiment should provide for more information on the phase velocity and its evolution given by the vorticity equation. This point is under current study.

7. Conclusions

We have studied a number of persistent episodes with vigorous above-normal baroclinic activity of a single wave m in northern hemisphere middle latitudes. Special emphasis was given to the packet of ultralong waves (e.g., $m = 2$ or $m = 3$) in order to show that their transient activity is much stronger than linear theory would have predicted. Note that the baroclinic activity of ultralong waves is normally (that is on average) comparable to that of typical synoptic scales (Table 1). We have shown that persistent episodes with vigorous above-normal baroclinic input $C(A_z A_m)$ develop like a baroclinic outbreak (BO) in most cases. Consequently, the baroclinic conversion $C(A_m K_m)$ and K_m are well developed at the same time. Our definition of BO-events depends on some more or less artificial threshold values; however, it enables us to study the most abnormal baroclinic input events belonging to one of two modes of baroclinic activity. These are: first a large number of periods with nearly normal baroclinic input $C(A_z A_m)$ and secondly a much smaller number of pronounced above-normal input during a longer time span. Despite the fact that the later episodes are relatively infrequent they provide for examples of outstanding dynamics. We have shown that the input pattern for kinetic energy is relatively simple then. The study of the underlying dynamics which causes and maintain the BO is a prerequisite for understanding the prototype of baroclinic activity which may operate as one of several prototypes in everyday atmospheric dynamics.

There are several potential drawbacks of the methods adopted in this paper. (i) Energetics alone does not describe the whole story of development. Phases of waves are also important and phase changes have to be studied carefully to complete the description of atmospheric states. This study is planned for the future. (ii) It is not clear whether the decomposition into zonal harmonics is optimal in describing interesting episodes of atmospheric development. A two-dimensional decomposition is utilized alternatively in a companion paper with some success. During major BO's for $m = 2$ it appears that only one meridional mode profits from the large energy input. This interesting result will be discussed in the companion paper. Alternatively, the study of packets of zonal waves may be favourable in neglecting unimportant details. (iii) Zonally averaged energy parameters are convenient but they say nothing about local events. Indeed we do not know whether we have studied strong local developments or the activity on a circumpolar scale. This is not really a crucial point since it is unlikely that well developed zonal waves $m = 1, \ldots, 3$ merely describe a modulation of basically localized effects. The signals found were so strong even after circumpolar averaging that our approach is justified à posterori.

Appendix A. List of symbols not explained in the text

$\langle\rangle$	: time mean
A_z	: $(p_B/g\sigma_0)\left[\frac{1}{2}\left\{\frac{\partial(\Phi - [\Phi]_{\varphi_1}^{\varphi_2}}{\partial p}\right\}^2\right]_{\varphi_1}^{\varphi_2}$
A_m	: $(p_B/g\sigma_0)\left[\frac{1}{2}\left\{\frac{\partial\Phi_m}{\partial p}\right\}^2\right]_{\varphi_1}^{\varphi_2}$
$\hat{K}_2$	: K_2 after (6b) but given by a regression model with $C(A_z A_m)(t)$ and conversions due to nonlinear wave-wave interactions as predictors. All variables are standardized to give zero mean and variance 1. The dimensional form is retrieved by: $X = \sigma_x \cdot \hat{X} + \langle X\rangle$; σ_x is the standard deviation of X
$J(X, Y)\|_m$	: Jacobian of X, Y projected onto wave m
λ,φ,t	: longitude, latitude, time
φ_A,φ_B	: boundaries of meridional averaging
β	: $df/d(a\varphi)$
f_0	: Coriolis parameter for $\varphi = 45°$N.
ϱ,α	: density, specific volume of dry air
p,Θ	: pressure, potential temperature
R	: gas constant (dry air)
c_p, c_v	: specific heat at constant pressure, constant volume
p_B	: 1000 mb pressure

Φ, ψ	: geopotential, streamfunction
ω	: $\mathrm{d}p/\mathrm{d}t$
$\bar{X}$	: zonal mean of $X = \left(\int_0^{2\pi} X \mathrm{d}\lambda\right)/2\pi$
X'	: deviation of X from $\bar{X}$
X_m	: field X projected onto zonal wavenumber m
a_m, b_m	: zonal Fourier—coefficients of zonal wave number m.
$a_{\tau,m}, b_{\tau,m}$	: a_m, b_m for the field $\tau = (1/g)h_m$.
Δp_i	: pressure increments: $\Delta p_1 = 200$ mb, $\Delta p_2 = 500$ mb
a	: earth radius
g	: earth gravity constant

Appendix B. Computing the ω- and heating-fields

We have to solve the quasi-geostrophic vorticity equation and the first law of thermodynamics for the ω- and heating-fields with tendencies computed from data. Our vertical data resolution (3 levels) is so poor that we decided to circumvent vertical derivatives whenever possible, and solve the problem iteratively. Moreover we pose it in two dimensional spectral form (subscripts m for zonal and n for meridional wavenumbers are dropped) by using the eigensolutions of the Laplacian for a channel on the sphere (for details see Egger and Schilling, 1983). The starting point is the ω-equation:

$$\begin{aligned}\partial^2\xi_j/\partial\pi^2 - \lambda^2 L_\mathrm{D}^2 \xi_j = &-(\lambda/f_0)^2 J(\psi_j, \Delta_j\Phi/\Delta_j\pi) \\ &+ (R\lambda^2/c_p\pi f_0^2)\mathrm{d}Q_j/\mathrm{d}t - \Delta_j J(\psi, \nabla^2\psi)/(\Delta_j\pi f_0) \\ &+ \beta/(\Delta_j\pi f_0) im\Delta_j\psi + (\nu\lambda^4 + \nu\lambda^2\Lambda^2/f_0)\frac{\Delta_j\psi}{\Delta_j\pi} = R_j,\end{aligned} \tag{B1}$$

$$\xi_j = \omega_j/p_\mathrm{B}$$

The layer index is j ($j = 1$: upper layer 300/500 mb; j = 2: lower layer 500/1000 mb). The abbreviations $\pi = p/p_\mathrm{B}$ and Δ_j = difference across layer j are used; $\lambda^2 = \lambda_{mn}^2$ is the eigenvalue of the mode under study and $L_\mathrm{D} = p_\mathrm{B}\sqrt{\sigma_0}/f_0$ denotes the Rossby radius of deformation. The right-hand side of (B1) is known, except for $\mathrm{d}Q/\mathrm{d}t$, the heating rate. For each layer, (B1) can be solved analytically with the assumption that R_j is constant across layer j. The boundary conditions for the solution of (B1) are:

$$\begin{aligned}&\xi_1(0.2) = 0; \quad \xi_2(1.0) = \\ &\quad -\varrho_\mathrm{B} g J(\psi_{1000}, h_\mathrm{B})|_{mn} - r_{\mathrm{ek}}\nabla^2\psi_{1000}, \\ &\xi_1(0.5) = \xi_2(0.5); \quad \partial\xi_1/\partial\pi(0.5) = \partial\xi_2/\partial\pi(0.5)\end{aligned} \tag{B2}$$

where h_B is the bottom topography and r_{ek} denotes Ekman-pumping. As a first guess we use $\mathrm{d}Q^{(1)}/\mathrm{d}t = 0$. The k-th iterative solution $\omega_j^{(k)}$ of (B1) is inserted into the first law:

$$\begin{aligned}(R/c_p\pi_j)\mathrm{d}Q_j/\mathrm{d}t = &(\partial/\partial t)\Delta_j\Phi/\Delta_j\pi + J(\psi_j, \Delta_j\Phi/\Delta_j\pi) \\ &- (f_0^2 L_\mathrm{D}^2)\xi_j\end{aligned} \tag{B3}$$

in order to find $\mathrm{d}Q_j^{(k+1)}/\mathrm{d}t$ and so on. The iteration converges fast. The only problem is with the diffusion parameter ν. Varying ν within reasonable limits shows that too small ν produces too low-valued ω (and heating) fields. Our results for ω were obtained for $\nu = 1.0 \times 10^6$ m^2/s which is acceptable for large scale flow (note that the diffusion represents the residue of the vorticity tendency not given explicitly by the other terms). In order to retrieve observed scalewise dissipation rates (e.g., Schilling, 1986) we are forced to set $\Lambda^2 = 50/a^2$ in (B1). Having computed the spectral coefficients for ω and dQ/dt in each layer we can recombine the series for the fields in $\lambda - \varphi$-space. Now we can form energy conversions for restricted φ-belts, etc.

Appendix C. Linear instability model

For a certain level we assume that $m = 2$ is projected onto linear eigenmodes n related to a suitably posed instability problem. The resulting amplitudes a_n are normalized in such a way that we have initially ($t = t_0$) the following partition of 'local' kinetic energy ($\delta_{n,n'}$ is the Kronecker symbol):

$$k_2(t_0) = k_{2,\mathrm{st}}\left\{1 + \sum_{n,n'}(2a_n p_{n,n'}\delta_{n,n'} + a_n a_{n'} q_{n,n'})\right\} \tag{C1}$$

and $q_{n,n} = 1$. The constants $p_{n,n'} \lesssim 1$ and $q_{n,n'} \lesssim 1$ incorporate phase relations and details stemming from the special mode structure. Let $n = 0$ be the most unstable mode with e-folding time T_e which gives an upper bound

$$k_2(t) \leqq k_{2,\mathrm{st}} \Big\{ 1 + \sum_{n,n'} (2a_n p_{n,n'} \delta_{n,n'} \exp(t/T_e) + a_n a_{n'} q_{n,n'} \exp(2t/T_e)) \Big\}. \tag{C2a}$$

In the most favourable case, the equality holds and the perturbation is completely represented by $n = 0$. In this case, we have

$$k_2(t_0) \leqq k_{2,\mathrm{st}}(1 + 2a_0 + a_0^2); \qquad \varepsilon^2 = k_2(t_0)/k_{2,\mathrm{st}}; \qquad a_0 = \varepsilon - 1, \tag{C2b}$$

if $p_{0,0} \leqq 1$. These relations hold for all levels. After integration over the flow domain the total kinetic energy $K_2(t)$ retains the same form as (C2b), (C2a):

$$K_2(t) = K_{2,\mathrm{st}}[1 + 2a_0 \exp(t/T_e) + a_0^2 \exp(2t/T_e)]; \qquad \varepsilon^2 = K_2(t_0)/K_{2,\mathrm{st}}; \qquad a_0 = \varepsilon - 1; \tag{C3}$$

if the representative perturbation amplitude a_0 is now defined by $\varepsilon - 1$ (by Schwarz's inequality, it is guaranteed that a_0 is larger than the domain-averaged amplitude).

After a time Δt we observe $K_2(t_0 + \Delta t)$ yielding after (C2a), (C3):

$$T_e \leqq \Delta t / \ln \{[\varepsilon\sqrt{(K_2(t_0 + \Delta t)/K_2(t_0))} - 1]/[\varepsilon - 1]\}. \tag{C4}$$

8. Acknowledgments

I wish to thank two anonymous reviewers for several valuable ideas and suggestions which have improved the presentation considerably.

REFERENCES

Bengtsson, L. 1978. Growth rate and vertical propagation of the initial error in baroclinic models. *Tellus 30*, 323–334.

Brown, J. A. 1969. A numerical investigation of hydrodynamic instability and energy conversions in the quasi-geostrophic atmosphere, Part II. *J. Atmos. Sci. 26*, 366–375.

Chen, T. C., Hansen, A. R. and Tribbia, J. J. 1981. A note on the release of available potential energy. *J. Meteorol. Soc. Japan 59*, 355–359.

Chen, T. C. and Shukla, J. 1983. Diagnostic analysis and spectral energetics of a blocking event in the GLAS climate model simulation. *Mon. Wea. Rev. 111*, 3–22.

Dole, R. M. 1986. Persistent anomalies of the extratropical northern hemisphere wintertime circulation: Structure. *Mon. Wea. Rev. 114*, 178–207.

Egger, J. and Schilling, H.-D. 1983. On the theory of the longterm variability of the atmosphere. *J. Atmos. Sci. 40*, 1073–1085.

Farrell, B. 1985. Transient growth of damped baroclinic waves. *J. Atmos. Sci. 42*, 2718–2727.

Fischer, G. 1984. Spectral energetics analysis of blocking events in a general circulation model. *Contrib. Atmos. Phys. 57*, 183–200.

Frederiksen, J. S. 1978. Baroclinic instability of zonal flows and planetary waves in multi-level models on a sphere. *J. Atmos. Sci. 35*, 2320–2335.

Gall, R. 1976. The effects of released latent heat in growing baroclinic waves. *J. Atmos. Sci. 33*, 1686–1701.

Hansen, A. R. 1986. Observational characteristics of atmospheric characteristics of atmospheric planetary waves with bimodal amplitude distribution. *Adv. Geophys.* (ed. by R. Benzi, B. Saltzman and A. Wiin-Nielsen), *29*, 101–133.

Hansen, A. R. and Chen, T. C. 1982. A spectral energetics analysis of atmospheric blocking. *Mon. Wea. Rev. 110*, 1146–1165.

Hansen, A. R. and Sutera, A. 1984. A comparison of the spectral energy and enstrophy budgets of blocking versus nonblocking periods. *Tellus 36A*, 52–63.

Itoh, H. 1983. An observational study on the amplification of planetary waves in the troposphere. *J. Meteorol. Soc. Japan 61*, 568–589.

Kubota, S. 1959. Numerical analysis of the energetical structure of the atmosphere over the northern hemisphere. *Pap. Meteorol. Geophys. 10*, 1–33.

Metz, W. 1986. Transient cyclone-scale vorticity forcing of blocking highs. *J. Atmos. Sci. 43*, 1467–1483.

Oerlemans, J. 1981. An observational study of the upward sensible heat flux by synoptic-scale transients. *Tellus 32*, 6–14.

Sasamori, T. and Youngblut, C. E. 1981. The nonlinear effects of transient and stationary eddies on the winter mean circulation. Part II: The stability of stationary waves. *J. Atmos. Sci. 38*, 87–96.

Schilling, H.-D. 1982. A numerical investigation of the dynamics of blocking waves in a simple two-level model. *J. Atmos. Sci. 39*, 998–1017.

Schilling, H.-D. 1984. Baroclinic instability of ultralong waves, Part II: Nonlinear baroclinic outburst episodes. *Contr. Atmos. Phys. 57*, 150–168.

Schilling, H.-D. 1986. On atmospheric blocking types and blocking numbers. *Adv. Geophys.* (ed. by R. Benzi, B. Saltzman and A. Wiin-Nielsen), *29*, 71–99.

Schilling, H.-D. 1987. Observed baroclinic energy conversions in wavenumber domain for 3 winters: A time series analysis. *Mon. Wea. Rev. 115*, 520–538.

Simpson, R. W. and Downey, W. K. 1975. The effect of a warm mid-latitude sea surface anomaly on a numerical simulation of the general circulation of the southern hemisphere. *Q. J. R. Meteorol. Soc. 101*, 847–867.

Smith, R. K. 1974. On limit cycles and vacillating baroclinic waves. *J. Atmos. Sci. 31*, 2008–2011.

Tomatsu, K. 1979. Spectral energetics of the troposphere and lower stratosphere. *Adv. Geophys. 21*, 289–405.

Tsay, C.-Y. and Kao, S.-K. 1978a. Linear and nonlinear contributions to the growth and decay of the large-scale atmospheric waves and jet stream. *Tellus 30*, 1–14.

Tsay, C.-Y. and Kao, S.-K. 1978b. Contributions to the growth and decay of large-scale eddy available potential energy. *Tellus 30*, 383–391.